



Cite this: *New J. Chem.*, 2018, 42, 19521

Ionic liquid/ether-plasticized quasi-solid-state electrolytes for long-life lithium–oxygen cells†

Chongjia Zhu,^a Qiushi Sun,^a Jian Xie,^{ib}*^{ab} Yuan Jin,^c Kangyan Wang,^c Zhen Chen,^d Jian Tu,^d Gaoshao Cao*^b and Xinbing Zhao^{ib}^{ab}

Rechargeable lithium–oxygen (Li–O₂) cells have aroused great attention due to their high theoretical energy density. However, a great challenge remains for the practical applications of Li–O₂ cells. One of the obstacles is the instability of the Li anode with organic electrolytes, even for relatively stable ether-based electrolytes. In this work, a quasi-solid state electrolyte, composed of a polymer, an inorganic ceramic electrolyte, Li salt and a plasticizer, was prepared. The quasi-solid state electrolyte plasticized by a hybrid of an ether and ionic liquid exhibits a stable interfacial contact with the metallic Li anode. At a limited capacity of 1000 mA h g⁻¹, the Li–O₂ cell with the quasi-solid-state electrolyte can be stably cycled for 196 cycles at 400 mA g⁻¹. The good cycling stability of the cell can be attributed to the stable metallic Li/electrolyte interface enabled by the F-containing protective layer formed *in situ* from the decomposition of the ionic liquid during cycling. This work provides a new design of solid state electrolytes for long-life Li–O₂ cells.

Received 7th July 2018,
Accepted 22nd October 2018

DOI: 10.1039/c8nj03389g

rsc.li/njc

Introduction

With the rapid development of grid energy storage and electric vehicle applications, traditional lithium-ion cells are unable to meet the demand in future, which necessitates researchers to exploit the next-generation lithium secondary cell with high energy density by using either high-capacity electrodes or solid electrolytes.^{1–3} Recently, rechargeable lithium–oxygen (Li–O₂) cells have aroused great interest due to the high theoretical energy density of 3505 W h kg⁻¹, rather higher than that of LiCoO₂-based cells.^{4–13} Furthermore, in Li–O₂ cells, the positive active material is oxygen, which can be obtained from air, so as to reduce the cost of the cells. However, the practical applications of Li–O₂ cells still face some considerable challenges, for example, those related to organic electrolytes. For the organic

Li–O₂ cell systems, the liquid organic electrolytes suffer from easy inflammability, explosion and volatilization, which will lead to serious safety issues.^{14–17}

Using solid state electrolytes instead of organic electrolytes provides an ideal strategy to solve this problem.^{18,19} Solid state electrolytes include inorganic solid electrolytes and polymer solid electrolytes.²⁰ A few inorganic solid electrolytes have high ionic conductivity and high anodic stability.^{21,22} Moreover, some inorganic solid state electrolytes can exist stably at high temperature and in a hostile environment.²³ By using inorganic solid state electrolytes to replace the liquid electrolyte and the separator in Li–O₂ cells, the crossover of O₂, CO₂ and H₂O in the cathode to the Li anode can be avoided or largely reduced, bringing about increased cycle life of the cells.²⁴ However, the interfacial resistance between inorganic electrolytes and electrodes is large. In addition, the mechanical properties of the inorganic solid electrolytes are usually poor. All of these limit their practical applications. In contrast, for the polymer solid electrolytes, the mechanical properties are outstanding which makes the manufacture easy.^{25,26} Therefore, it is expected that the interfacial performance and the mechanical properties of the electrolytes should be improved by combining polymer and inorganic solid electrolytes.^{27,28}

Here, we designed a quasi-solid state electrolyte (QSSE) with an ionic liquid/ether as the plasticizer. The QSSE consists of four components, including a polymer solid electrolyte matrix, a ceramic electrolyte additive, lithium salt and a plasticizer, where the polymer solid electrolyte matrix is composed of poly(propylene carbonate) (PPC)²⁹ and poly(vinylidene fluoride-hexafluoropropylene)

^a State Key Laboratory of Silicon Materials, School of Materials Science and Engineering, Zhejiang University, Hangzhou 310027, P. R. China.
E-mail: xiejian1977@zju.edu.cn, gsciao@zju.edu.cn; Fax: +86 571 87952181;
Tel: +86 571 87951451

^b Key Laboratory of Advanced Materials and Applications for Batteries of Zhejiang Province, Hangzhou 310027, P. R. China

^c Zotye Automobile Corporation Limited, Hangzhou 310018, P. R. China

^d LI-FUN Technology Corporation Limited, Zhuzhou 412000, P. R. China

† Electronic supplementary information (ESI) available: XRD and SEM of LATP, XRD of the dry solid membrane, SEM image of IrO₂/MnO₂ on carbon cloth, photo and XRD of the failed Li anode, cycling performance of the re-assembled cell with fresh Li, rate capability of the cells with different QSSEs, the initial voltage profiles of Li–O₂ cell with TEGDME-plasticized QSSE, Nyquist plot of QSSE, photo of Li anode covered by PI film, and structural formulas of PMIMTFSI and P(VDF-HFP). See DOI: 10.1039/c8nj03389g

P(VDF-HFP).³⁰ PPC is a polymer that makes the electrolyte flexible. However, only the PPC matrix is unstable because the QSSE will decompose in the presence of the plasticizer for long-time cycling of the Li–O₂ cells. Li_{1.3}Al_{0.3}Ti_{1.7}(PO₄)₃ (LATP) was used as a ceramic electrolyte additive, since it has a high ionic conductivity.^{31,32} The mechanical strength and ionic conductivity of the polymer solid electrolyte will be improved by adding LATP nanoparticles. The plasticizer is composed of ethylene glycol dimethyl ether (TEGDME) and 1-propyl-3-methylimidazolium bis(trifluoromethylsulfonyl)imide (PMIMTFSI), the addition of which not only improves the ionic conductivity of the QSSE but also reduces the interface impedance between the QSSE and electrodes.

Experimental section

Preparation of LATP nanoparticles

LATP nanoparticles were synthesized by a modified sol-gel method as previously reported.^{33,34} First, 19.6 mL of 25 wt% ammonia water (Sinopharm Chemical Reagent Co., Ltd, China) was added dropwise to 10 mL of titanium(IV) isopropoxide (97%, Sigma-Aldrich) with magnetic stirring for 1 h. The precipitate was filtrated and dispersed into deionized (DI) water (40 mL) followed by the addition of 80 mL of 1 M aqueous solution of oxalic acid ($\geq 99.5\%$, Shanghai Mei Xing Chemical Co., Ltd, China). The mixture was stirred until the precipitate was completely dissolved. After this, LiNO₃ (1.832 g, analytical reagent (AR), Shanghai Feng Shun Fine Chemical Co., Ltd, China), Al(NO₃)₃·6H₂O (2.212 g, 98%, Alfa Aesar) and (NH₄)₂HPO₄ (7.751 g, AR, Sinopharm Chemical Reagent Co., Ltd, China) were added into the above solution with stirring for 12 h to get the LATP precursor solution. Second, a surfactant, cetyltrimethylammonium bromide (CTAB, 6 g, AR, Sinopharm Chemical Reagent Co., Ltd, China), was dissolved into 40 mL of anhydrous alcohol (AR, Sinopharm Chemical Reagent Co., Ltd, China) with magnetic stirring at 40 °C for 2 h, and then the solution was added into the LATP precursor solution with vigorous stirring. Subsequently, the solution was tempered in an oil bath at 80 °C until the solvent was completely evaporated to form a transparent jelly. Finally, the jelly was heated to 600 °C at 2 °C min⁻¹ in an OTF-1200X tube furnace (Hefei Kejing Materials Technology Co., Ltd, China) under an Ar atmosphere, kept at that temperature for 12 h, and cooled to room temperature naturally.

Preparation of QSSE membrane

The QSSE was prepared by a one-pot method. First, 0.8 g of PPC (average molecular weight 5000, Sigma-Aldrich) and 0.8 g of P(VDF-HFP) (average molecular weight 110 000, Sigma-Aldrich) were added into 50 mL of *N*-methyl-2-pyrrolidone (NMP, AR, Sinopharm Chemical Reagent Co., Ltd, China). The mixture was heated in an oil bath at 80 °C for 3 h under strong stirring until the polymers were completely dissolved. Second, bis(trifluoromethane) sulfonamide lithium salt (LITFSI, 99.95%, Sigma-Aldrich, 0.32 g) and LATP powder (0.32 g) were added into the above solution with magnetic stirring for 24 h. Then,

the viscous liquid that contains polymers, LITFSI and LATP was poured into Teflon containers and dried in an electric oven at 60 °C first in air for 48 h and then in a vacuum for another 24 h to get solid electrolyte membranes. Two kinds of polymers were used for the easy formation of stable membranes. Finally, three types of QSSE membranes were obtained by immersing the solid membranes in three different solutions, namely 1 M LiClO₄ (99.99%, Sigma-Aldrich) in TEGDME ($\geq 99.0\%$, Sigma-Aldrich), PMIMTFSI ($\geq 98\%$, Sigma-Aldrich) and a hybrid (TEGDME : PMIMTFSI = 1 : 1, in volume), respectively, for 24 h and wiping off the excess liquid on the surface of the membranes.

Materials characterization

X-ray diffraction (XRD) patterns were collected using a Rigaku D/Max-2550pc powder diffractometer with Cu K α radiation ($\lambda = 1.541 \text{ \AA}$). X-ray photoelectron spectra (XPS) were recorded on a KRATOS AXIS ULTRA-DLD spectrometer with monochromatic Al K₂ radiation ($h\nu = 1486.6 \text{ eV}$). The morphology of the samples was observed by field-emission scanning electron microscopy (SEM) using an S-4800 microscope.

Electrochemical measurements

Coin-type cells were assembled in an argon-filled glove box using metallic lithium as the anode (AR, Sinopharm Chemical Reagent Co., Ltd, China), IrO₂/MnO₂ on carbon cloth as the cathode and the QSSE membrane as the electrolyte. The IrO₂/MnO₂ catalyst was prepared according to our previous report,³⁵ and the loading of IrO₂/MnO₂ on carbon cloth is around 0.4 mg cm⁻². The electrodes were dried at 80 °C in a vacuum overnight prior to cell fabrication. The cells were purged with pure O₂ for 10 min before the electrochemical measurements. Charge and discharge cycling was conducted using a Neware cell cycler (Shenzhen, China) between 2.0 and 4.5 V vs. Li/Li⁺. The specific capacity and current density were normalized to the total mass of IrO₂ and MnO₂. Electrochemical impedance spectroscopy (EIS) was acquired on a CHI660C (Chenhua, China) workstation by applying an AC voltage of 10 mV amplitude over a frequency range of 10⁻²–10⁵ Hz. The electrochemical measurements were all carried out at 25 °C.

Results and discussion

As seen in Fig. S1a (ESI[†]), phase-pure LATP was obtained after high-temperature firing. The particle size of LATP is in the nanoscale (Fig. S1b, ESI[†]). The photographs of the QSSE plasticized by TEGDME, PMIMTFSI and a hybrid (TEGDME : PMIMTFSI = 1 : 1, in volume) are shown in Fig. 1. All the QSSE membranes have a smooth surface and exhibit a flexible feature. For a typical dry solid membrane of 19 mm diameter and 0.4 mm thickness, the weight is around 100 mg. The weight of the membranes increases to 160, 200 and 170 mg after absorbing TEGDME, PMIMTFSI, and TEGDME/PMIMTFSI, respectively. This suggests that the P(VDF-HFP) and PPC are good matrices that absorb the plasticizers. The XRD patterns in Fig. S2 (ESI[†])

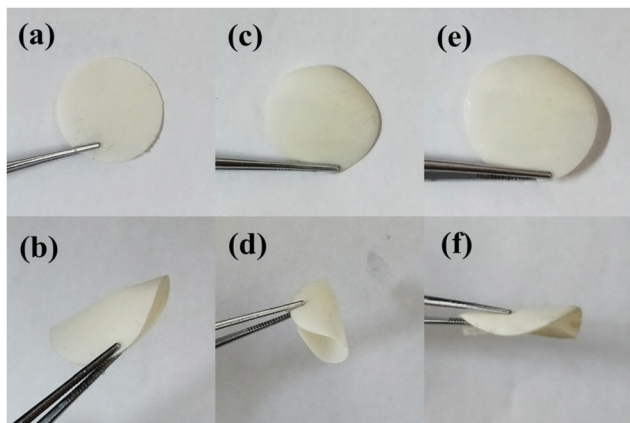


Fig. 1 Photos of QSSE plasticized by (a and b) TEGDME, (c and d) PMIMTFSI, and (e and f) the TEGDME/PMIMTFSI hybrid.

reveal the expected diffraction peaks of LATP of the dry solid membrane, while the broad hump at 20° (2θ) indicates the presence of PPC and P(VDF-HFP). Fig. 2 shows the SEM images of the dry solid membrane and the QSSE membranes with various plasticizers. Note that after immersion in the liquid electrolyte, all the membranes can retain the porous structure, which is favorable for rapid Li-ion transportation within the QSSE membranes.

Fig. 2 shows the voltage profiles and cycling performance of the Li–O₂ cells using the QSSE with a limited capacity of 1000 mA h g^{-1} at 400 mA g^{-1} between 2.0 and 4.5 V. The catalyst used was IrO₂/MnO₂ deposited on carbon cloth that exhibits a flake-like structure (Fig. S3, ESI[†]). The current density and specific capacity were calculated based on the total mass of MnO₂ and IrO₂ catalysts. The cycling performance of the Li–O₂ cells using three different QSSE membranes is compared as shown in Fig. 3a. Although the cell with the TEGDME-plasticized QSSE shows a relatively high terminal discharge voltage of over 2.8 V and a terminal charge voltage of slightly

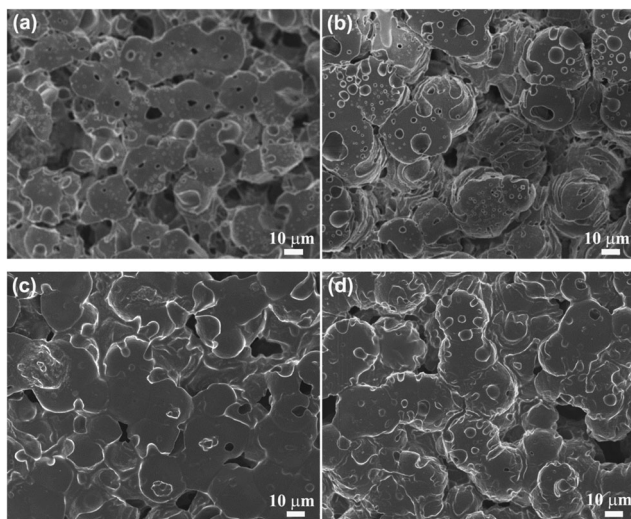


Fig. 2 SEM images of (a) dry solid membrane and QSSE membranes with (b) TEGDME, (c) PMIMTFSI and (d) TEGDME/PMIMTFSI plasticizers.

over 4.0 V during the initial cycles, the terminal charge voltage increases rapidly to 4.5 V after 90 cycles. Namely, with a limited capacity of 1000 mA h g^{-1} at 2.0–4.5 V, the reversible cycling of the cell can last only 90 cycles (Fig. 3a and b). During the initial cycles, the relatively low polarization can be attributed to the rapid transportation of Li ions in the TEGDME-plasticized QSSE and the QSSE/Li anode interface. Post-mortem characterization demonstrates that the originally shiny lithium plate has transformed into white powder (Fig. S4a, ESI[†]). The white powder is proved to be LiOH by XRD (Fig. S4b, ESI[†]). The cell was re-assembled using fresh Li and it can be stably cycled for another 80 cycles (Fig. S5, ESI[†]). The total cycle number can be increased to 239 cycles when the failed Li anode was replaced again (Fig. S5, ESI[†]). The results indicate that the QSSE membrane is relatively stable in the O₂ environment for long-term cycling, and that the failure of the Li anode contributes to the performance degradation of the cell, at least in part. Compared with the cell using the TEGDME-plasticized QSSE, the cell using PMIMTFSI-plasticized QSSE shows improved cycle life as seen in Fig. 3a and c. It is suggested that the improved cycling performance is due to the inhibited interfacial reaction between the Li anode and the electrolyte, which will be discussed below. As shown in Fig. 3a and d, the stable cycling of the cell can be extended up to 196 cycles when using the QSSE with the TEGDME/PMIMTFSI hybrid plasticizer. In this case, the Li-ion transportation and interfacial stability between the Li anode and the QSSE are assumed to be balanced. To highlight the good electrochemical performance of our cells, we compared the electrochemical performance of some Li–O₂ cells using solid electrolytes (Table S1, ESI[†]). As seen in the table, the electrochemical performance of our cell is among the best. The rate capability of the cells with different QSSEs was also tested as shown in Fig. S6 (ESI[†]). As the current density increases, the polarization increases and even the capacity cannot reach 1000 mA h g^{-1} , which is ascribed to the sluggish oxygen reduction reaction (ORR)/oxygen evolution reaction (OER) kinetics and low Li-ion transportation rate in the QSSE. In addition, the relatively high current density also contributes to the relatively low energy efficiency. Note that the cell with the TEGDME-plasticized QSSE exhibits a relatively high discharge terminal voltage of 2.86 V and a relatively low charge terminal voltage of 3.96 V in the initial cycle (Fig. S7, ESI[†]) although the polarization increases during cycling.

Fig. 4 shows the voltage profiles of the Li–O₂ cell with the QSSE plasticized by the TEGDME/PMIMTFSI hybrid at 400 mA g^{-1} in the full charge/discharge mode between 2.0 and 4.5 V. The first charge and discharge capacities in this mode are 1340 and 1844 mA h g^{-1} , respectively. The exact origin of the higher charge capacity in the first cycle is unclear but it may be related to electrolyte decomposition. After the first cycle, the charge capacity and discharge capacity are almost the same, indicating high reversibility of the cell. It should be noted that the capacity is not high even in this cycling mode at a moderate current density (400 mA g^{-1}) due to the relatively low Li-ion conductivity of $3.1 \times 10^{-4} \text{ S cm}^{-1}$ at room temperature

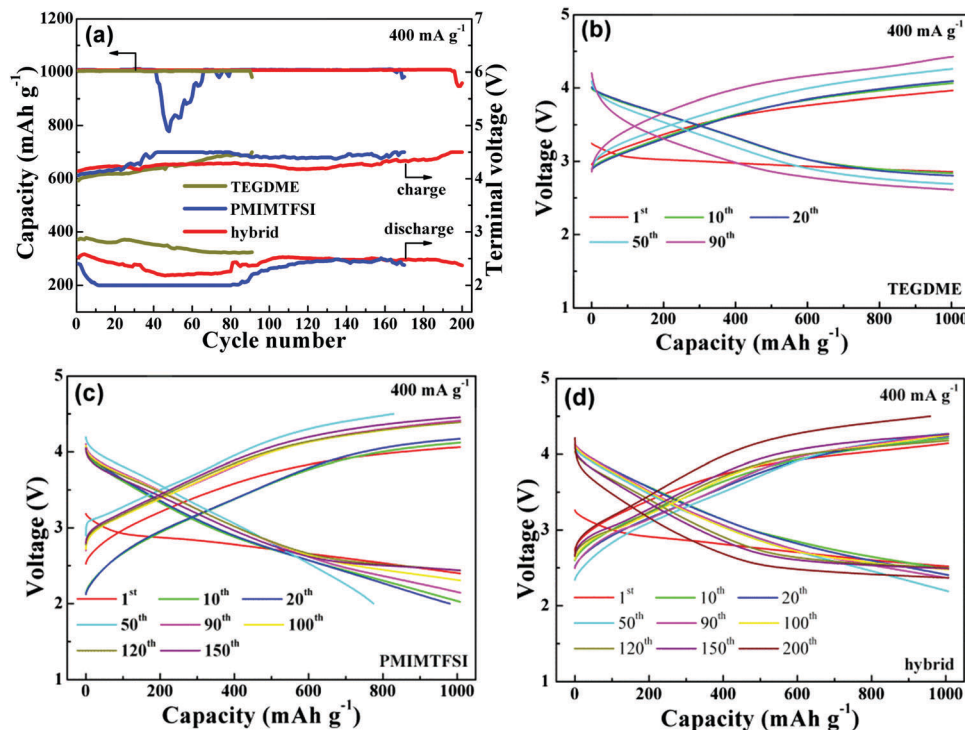


Fig. 3 Voltage profiles and cycling performance of Li–O₂ cells with a limited capacity of 1000 mA h g⁻¹ at 400 mA g⁻¹: (a) cycling performance of cells with three different QSSEs, and voltage profiles of cells using the QSSE plasticized by (b) TEGDME, (c) PMIMTFSI and (d) the TEGDME/PMIMTFSI hybrid.

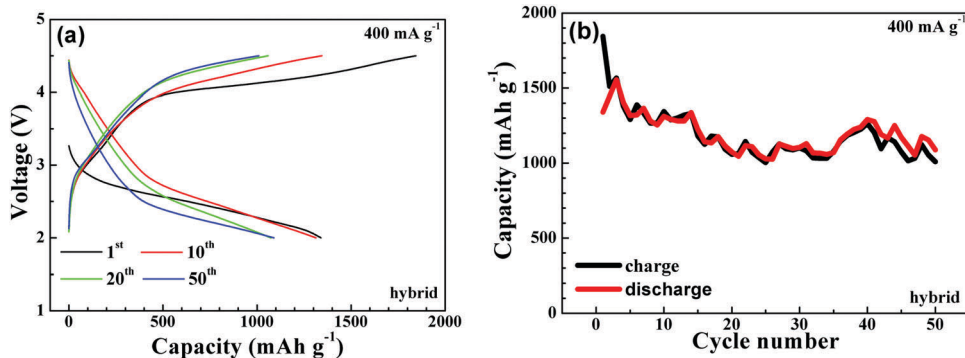


Fig. 4 (a) Voltage profiles and (b) cycling performance of the Li–O₂ cell with the QSSE plasticized by the TEGDME/PMIMTFSI hybrid at 400 mA g⁻¹ between 2.0 and 4.5 V.

(Fig. S8, ESI[†]) determined by EIS.³⁶ Even so, the cell can be cycled for 50 cycles, where the capacity is over 1000 mA h g⁻¹ in this relatively stringent cycling mode. As expected, the conductivity of the QSSE with the TEGDME/PMIMTFSI hybrid is between that with TEGDME and PMIMTFSI (Fig. S8, ESI[†]).

To better understand the reason why Li–O₂ cells that use different QSSEs exhibit different electrochemical performances, the Li anodes were checked by XRD after the 1st, 20th, and 50th cycle as shown in Fig. 5. Here, polyimide (PI) films were used to prevent the lithium anodes from exposure to air (Fig. S9, ESI[†]). Fig. 5a shows that after the first cycle, there is no obvious difference among the three lithium anodes from the three cells, and LiOH peaks are barely observed. After 20 cycles, almost no LiOH is visible for the Li anode from the cell that

uses PMIMTFSI-plasticized QSSEs (Fig. 5b). In contrast, a small diffraction peak at 32.5° (2θ) appears for the Li anode from the cell with the TEGDME-plasticized QSSE, which indicates the formation of LiOH. As previously reported, TEGDME is chemically/electrochemically unstable towards metallic lithium.³⁷ In the case of using the TEGDME/PMIMTFSI hybrid, only a small peak is seen at 32.5° (2θ), suggesting that the formation of LiOH is minor. Fig. 5c demonstrates that the interfacial reaction between Li and TEGDME becomes significant as the cycling proceeds, which agrees well with the performance degradation of the cell. In comparison, the LiOH peak is hardly seen in the case of using the PMIMTFSI plasticizer. It seems that the introduction of PMIMTFSI prevents the reaction between TEGDME and the Li anode, evidenced from the small LiOH

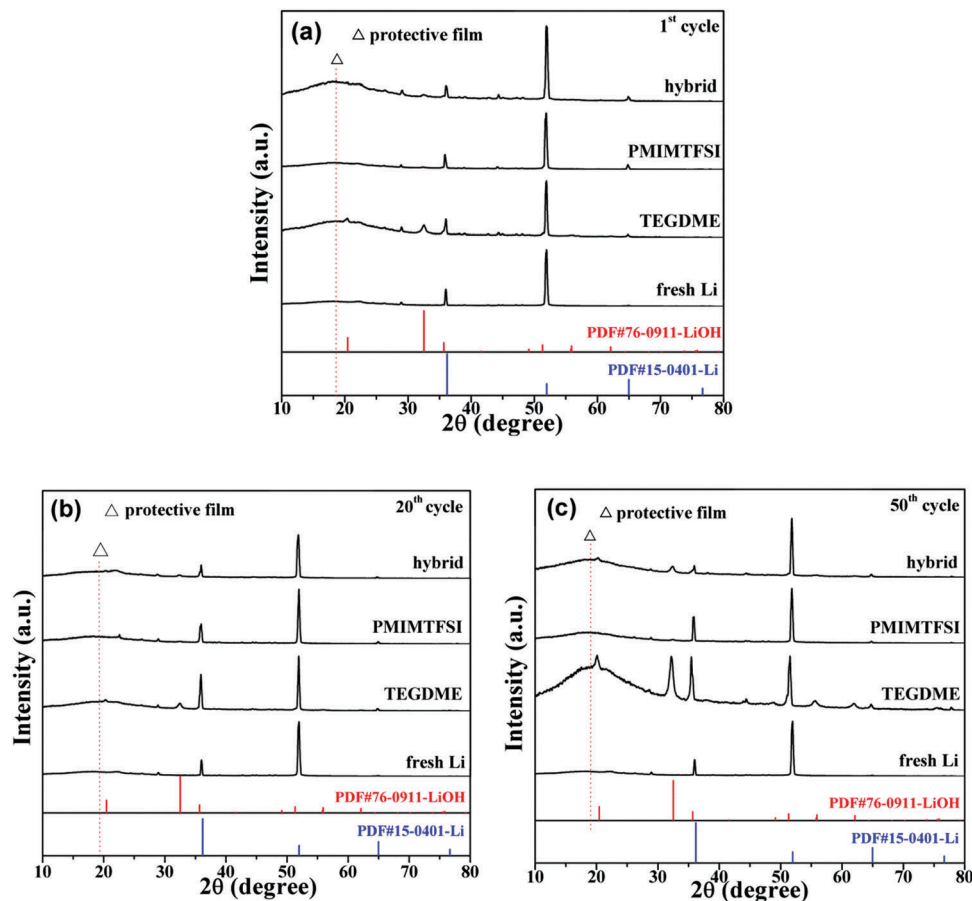


Fig. 5 XRD patterns of the Li anodes after the (a) first charge, (b) 20th charge, and (c) 50th charge with a limited capacity of 1000 mA h g^{-1} at 400 mA g^{-1} .

peak for the hybrid plasticizer. The results suggest that the ionic liquid PMIMTFSI plays a critical role in stabilizing the Li anode.

To further identify the mechanism for the improved stability of the Li anode by using PMIMTFSI, XPS analyses of Li anodes after 50 cycles were performed as shown in Fig. 6. The C–C bond at 284.6 eV is used to calibrate the binding energy spectrum for the XPS analyses. The survey spectrum shows that each Li tablet surface contains elements of Li, C, N, O and F (Fig. 6a). An obvious difference in Fig. 6a is the peak intensity of F1s when different plasticizers were used. It is obvious that the strong F1s peak in the cases of PMIMTFSI and the hybrid is closely related to the use of F-containing ionic liquid, although the LITFSI salt also contains the F element. From the XPS and XRD results, it can be concluded that the fluoride *in situ* formed from the decomposition of the ionic liquid prevents the reaction between lithium and TEGDME and precludes the further reaction between lithium and PMIMTFSI. As a result, the cycling performance of the Li–O₂ cells is enhanced due to the stabilized Li/electrolyte interface. Fig. 6b and c show the F1s and C1s spectra of the Li tablets from the cells with the QSSE plasticized by the TEGDME/PMIMTFSI hybrid. The band at 688.9 eV is attributed to –CF₃ groups (Fig. 6b). The C1s spectrum is fitted by five peaks with binding energies of 284.6, 286.4, 289.9, 290.4 and 292.8 eV, which are attributed to the C–C group, the C=O group, the –(CF₂–CH₂)_n group, the –(CF₂–CF₂)_n group and the

–CF₃ group, respectively. The F1s and C1s peaks at 688.9 and 292.8 eV are well in accordance with the –CF₃ group, which indicates that the fluoride containing the –CF₃ group is effective in protecting the Li anode. It is suggested that the –CF₃ group originates mainly from the decomposition of PMIMTFSI (Fig. S10a, ESI†). During the charge/discharge cycling, the S–N and S–C bonds from the TFSI anion break which produces SO₂ and CF₃ species and an NSO₂CF₃–Li complex.³⁸ The SO₂ and CF₃ species were rapidly atomized and incorporated into the lithium anode and the NSO₂CF₃–Li complex was unstable, which is eventually decomposed into N, SO₂, and CF₃ species,³⁸ leading to the formation of the –CF₃-containing compound. The –(CF₂–CH₂)_n group originates from the P(VDF–HFP) (Fig. S10b, ESI†).

Soft-pack cells were also assembled with a cathode size of 2.5 cm × 2.5 cm. The cathode, the QSSE membrane (TEGDME/PMIMTFSI hybrid plasticizer) and the Li anode were laminated and sealed in a polyethylene bag with some small holes punched on the cathode for O₂ flowing (Fig. 7). The soft-pack cell was sandwiched between two Teflon plates to enable good contact of the cell components. The Teflon-sandwiched cell was then sealed in a plastic bottle filled with pure O₂ for electrochemical tests (Fig. 7c). Fig. 7b shows the voltage profiles of the soft-pack Li–O₂ cell at 200 mA g^{−1} with a limited capacity of 1000 mA h g^{−1}. Fig. 6c also shows that the soft-pack Li–O₂ cell powers light-emitting diodes (LED).

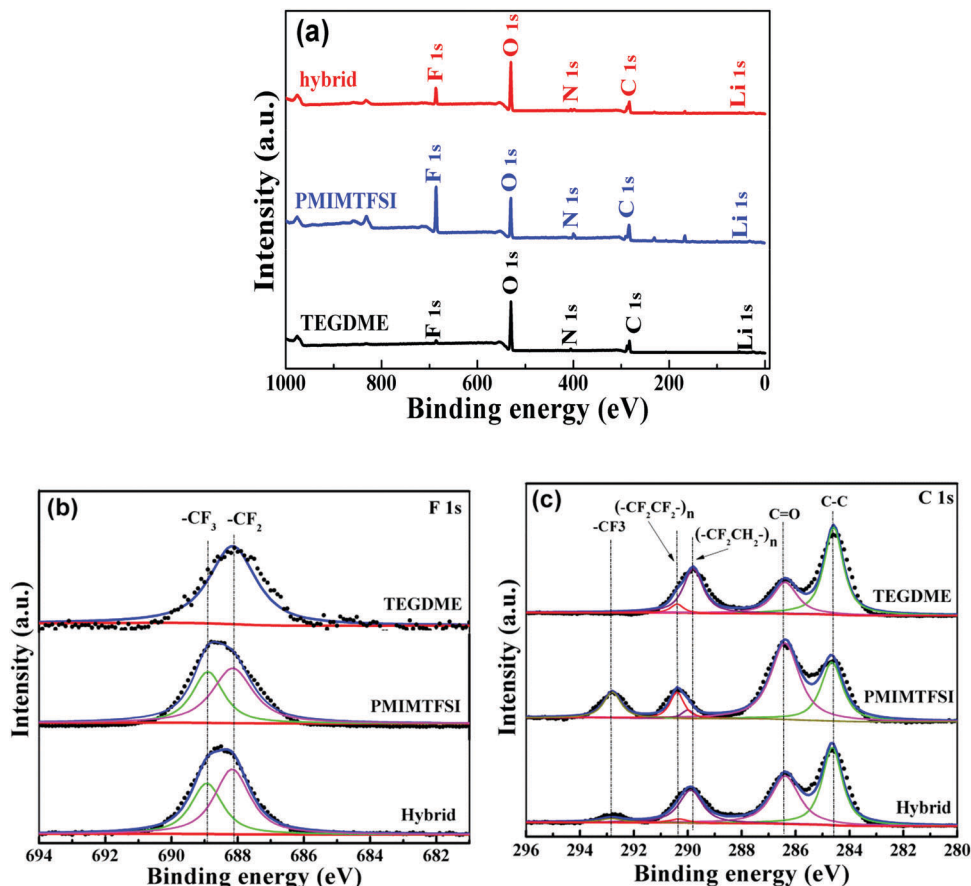


Fig. 6 (a) XPS survey of the Li anodes after 50 cycles using the QSSE with three different plasticizers, and (b) F1s and (c) C1s spectra of the Li anode using the QSSE with the TEGDME/PMIMTFSI hybrid plasticizer.

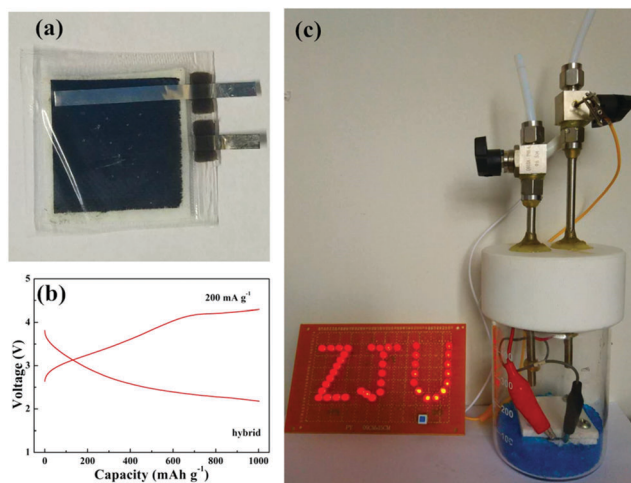


Fig. 7 Photos of (a) a soft-pack Li–O₂ cell using the QSSE with the TEGDME/PMIMTFSI hybrid plasticizer, (b) voltage profiles of the soft-pack at 200 mA g⁻¹, and (c) the device containing O₂ to test the soft-pack Li–O₂ cell that powers LEDs.

Conclusions

In summary, we designed a QSSE, which is composed of the P(VDF-HFP)/PPC polymer matrix, the Li_{1.3}Al_{0.3}Ti_{1.7}(PO₄)₃ inorganic

electrolyte additive, the LITFSI salt and the TEGDME/PMIMTFSI hybrid plasticizer. The QSSE shows good flexibility, satisfactory strength and acceptable room-temperature Li-ion conductivity. The Li–O₂ cell assembled with the QSSE shows good cycling performance. The cell can maintain stable cycling up to 196 cycles at 400 mA g⁻¹ with a limited capacity of 1000 mA h g⁻¹. In a full charge/discharge mode at 400 mA g⁻¹ between 2 and 4.5 V, the cell can be cycled for 50 cycles with a capacity over 1000 mA h g⁻¹. The fluoride containing –CF₃ group which is *in situ* formed from the decomposition of PMIMTFSI protects the Li anode from the reactions with TEGDME, bringing about the long cycle life of the Li–O₂ cells. This work provides a promising design of quasi-solid state electrolytes compatible with the Li anode.

Conflicts of interest

There are no conflicts to declare.

Acknowledgements

This work was supported by the National Natural Science Foundation of China (No. 51572238), The Zhejiang Provincial Natural Science Foundation of China under Grant no. LY19E020013,

the Strategic Emerging Industry Project of Hunan Province (2016GK4030), and the Joint Research Project with Zotye Automobile Corporation Limited (P-ZH-2018-003).

References

- W. S. Weng, J. Lin, Y. C. Du, X. F. Ge, X. S. Zhou and J. C. Bao, *J. Mater. Chem. A*, 2018, **6**, 10168–10175.
- X. Liu, Y. C. Du, L. Y. Hu, X. S. Zhou, Y. F. Li, Z. H. Dai and J. C. Bao, *J. Phys. Chem. C*, 2015, **119**, 5848–5854.
- L. Chen, Y. T. Li, S. P. Li, L. Z. Fana, C. W. Nan and J. B. Goodenough, *Nano Energy*, 2018, **46**, 176–184.
- K. M. Abraham and Z. Jiang, *J. Electrochem. Soc.*, 1996, **143**, 1–5.
- Z. Q. Peng, S. A. Freunberger, Y. H. Chen and P. G. Bruce, *Science*, 2012, **337**, 563–566.
- M. M. Ottakam Thotiyil, S. A. Freunberger, Z. Q. Peng, Y. H. Chen, Z. Liu and P. G. Bruce, *Nat. Mater.*, 2013, **12**, 1050–1056.
- K. Song, D. A. Agyeman, M. Park, J. Yang and Y. M. Kang, *Adv. Mater.*, 2017, **29**, 1606572.
- P. Zhang, Y. Zhao and X. B. Zhang, *Chem. Soc. Rev.*, 2018, **47**, 2921–3004.
- P. Tan, B. Chen, H. R. Xu, H. C. Zhang, W. Z. Cai, M. Ni, M. L. Liu and Z. P. Shao, *Energy Environ. Sci.*, 2017, **10**, 2056–2080.
- Z. Ma, X. X. Yuan, L. Li, Z. F. Ma, D. P. Wilkinson, L. Zhang and J. J. Zhang, *Energy Environ. Sci.*, 2015, **8**, 2144–2198.
- M. Balaish, A. Kraytsberg and Y. Ein Eli, *Phys. Chem. Chem. Phys.*, 2014, **16**, 2801–2822.
- A. Kraytsberg and Y. Ein Eli, *J. Power Sources*, 2011, **196**, 886–893.
- J. S. Lee, S. T. Kim, R. G. Cao, N. S. Choi, M. L. Liu, K. T. Lee and J. Cho, *Adv. Energy Mater.*, 2011, **1**, 34–50.
- K. Xu, *Chem. Rev.*, 2014, **114**, 11503–11618.
- Z. Y. Lyu, Y. Zhou, W. R. Dai, X. H. Cui, M. Lai, L. Wang, F. W. Huo, W. Huang, Z. Hu and W. Chen, *Chem. Soc. Rev.*, 2017, **46**, 6046–6072.
- K. D. Cai, W. H. Pu, Y. Gao, J. B. Hou, C. S. Deng, C. Wang and Z. Q. Mao, *Int. J. Hydrogen Energy*, 2013, **38**, 11023–11027.
- J. Pan, H. P. Li, H. Sun, Y. Zhang, L. Wang, M. Liao, X. M. Sun and H. S. Peng, *Small*, 2018, **14**, 1703454.
- J. Yi, S. H. Guo, P. He and H. S. Zhou, *Energy Environ. Sci.*, 2017, **10**, 860–884.
- C. P. Yang, K. Fu, Y. Zhang, E. Hitz and L. B. Hu, *Adv. Mater.*, 2017, **29**, 1701169.
- A. Manthiram, X. W. Yu and S. F. Wang, *Nat. Rev. Mater.*, 2017, **2**, 16103.
- Y. J. Liu, P. He and H. S. Zhou, *Adv. Energy Mater.*, 2018, **8**, 1701602.
- L. P. Yue, J. Ma, J. J. Zhang, J. W. Zhao, S. M. Dong, Z. H. Liu, G. L. Cui and L. Q. Chen, *Energy Storage Mater.*, 2016, **5**, 139–164.
- Q. P. Guo, Y. Han, H. Wang, S. Z. Xiong, W. W. Sun, C. M. Zheng and K. Xie, *J. Phys. Chem. C*, 2018, **122**, 10334–10342.
- P. He, T. Zhang, J. Jiang and H. S. Zhou, *J. Phys. Chem. Lett.*, 2016, **7**, 1267–1280.
- W. H. Hou, C. Y. Chen, C. C. Wang and Y. H. Huang, *Electrochim. Acta*, 2003, **48**, 679–690.
- J. J. Bao, C. Tao, R. Yu, M. H. Gao, Y. P. Huang and C. H. Chen, *J. Appl. Polym. Sci.*, 2017, **134**, 45554.
- J. Yi, Y. Liu, Y. Qiao, P. He and H. S. Zhou, *ACS Energy Lett.*, 2017, **2**, 1378–1384.
- X. Zhang, T. Liu, S. F. Zhang, X. Huang, B. Q. Xu, Y. H. Lin, B. Xu, L. L. Li, C. W. Nan and Y. Shen, *J. Am. Chem. Soc.*, 2017, **139**, 13779–13785.
- J. Y. Sun, N. Zhao, Y. Q. Li, X. X. Guo, X. F. Feng, X. S. Liu, Z. Liu, G. L. Cui, H. Zheng, L. Gu and H. Li, *Sci. Rep.*, 2017, **7**, 41217.
- Y. S. Zhu, Y. Q. Yang, L. J. Fu and Y. P. Wu, *Electrochim. Acta*, 2017, **224**, 405–411.
- B. Key, D. J. Schroeder, B. J. Ingram and J. T. Vaughey, *Chem. Mater.*, 2012, **24**, 287–293.
- C. Cao, Z. B. Li, X. L. Wang, X. B. Zhao and W. Q. Han, *Front. Energy Res.*, 2014, **2**, 25.
- M. Kotobuki and M. Koishi, *Ceram. Int.*, 2013, **39**, 4645–4649.
- O. L. Andreev, K. V. Druzhinin, P. Y. Shevelin and N. N. Batalov, *Ionics*, 2013, **19**, 33–39.
- C. Tang, P. C. Sun, J. Xie, Z. C. Tang, Z. X. Yang, Z. X. Dong, G. S. Cao, S. C. Zhang, P. V. Braun and X. B. Zhao, *Energy Storage Mater.*, 2017, **9**, 206–213.
- Y. H. Liu, X. Y. Yu, Y. J. Fang, X. S. Zhu, J. C. Bao, X. S. Zhou and X. W. Lou, *Joule*, 2018, **2**, 725–735.
- R. S. Assary, J. Lu, P. Du, X. Y. Luo, X. Y. Zhang, Y. Ren, L. A. Curtiss and K. Amine, *ChemSusChem*, 2013, **6**, 51–55.
- J. B. Haskins, H. Yildirim, C. W. Bauschlicher Jr and J. W. Lawson, *J. Phys. Chem. C*, 2017, **121**, 28235–28248.